

## Vortex Content of $SU(2)$ Calorons and Multi-Calorons

---

### Bo Zhang\*

*Institut für Theoretische Physik, Universität Regensburg, D-93040 Regensburg, Germany*

*E-mail: [bo1.zhang@physik.uni-regensburg.de](mailto:bo1.zhang@physik.uni-regensburg.de)*

### Falk Bruckmann

*Institut für Theoretische Physik, Universität Regensburg, D-93040 Regensburg, Germany*

*E-mail: [falk.bruckmann@physik.uni-regensburg.de](mailto:falk.bruckmann@physik.uni-regensburg.de)*

### Ernst-Michael Ilgenfritz

*Institut für Theoretische Physik, Ruprecht-Karls-Universität Heidelberg, D-69120 Heidelberg, Germany*

*Institut für Physik, Humboldt-Universität, D-12489 Berlin, Germany*

*E-mail: [ilgenfri@physik.hu-berlin.de](mailto:ilgenfri@physik.hu-berlin.de)*

We use Laplacian Center Gauge to reveal the vortex content of single  $SU(2)$  calorons and multi-caloron systems at different holonomies. The vortex surfaces in a single  $SU(2)$  caloron consist of two parts that are induced by the constituent dyon charges and by the twist between the dyons, respectively. The latter part percolates in a caloron ensemble at maximal nontrivial holonomy. This finding fits perfectly in the confinement scenario of vortices and shows that calorons are suitable to facilitate the vortex confinement mechanism.

*The XXVII International Symposium on Lattice Field Theory - LAT2009*

*July 26-31 2009*

*Peking University, Beijing, China*

---

\*Speaker.

## 1. Caloron, Monopole and Vortex

Topological excitations are candidates for the mechanism for nonperturbative effects in QCD including confinement and chiral condensate. The most intensively examined topological excitations are instantons, magnetic monopoles and center vortices. Instantons are solutions of the equation of motion, thus can be introduced into QCD in a semiclassical approach. It can explain the chiral condensate naturally through the (quasi) zero mode, but confinement remained unexplained with instantons. On the other hand, Abelian monopoles and vortices are not of semiclassical nature, but represent defects of codimension 3 and 2, respectively, that remain after gauge fixings and projections. They can explain confinement, and some quantitative studies [1] show that they are a prerequisite for the occurrence of topological charge in general.

Calorons [2, 3, 4] are generalizations of instantons at finite temperature. The asymptotic Polyakov loop plays a key role in determining the properties of calorons. In  $SU(2)$ , we parameterize it as  $P(\vec{x} \rightarrow \infty) = e^{2\pi i \omega \sigma_3}$  with the holonomy parameter  $\omega$ . A nontrivial holonomy caloron ( $\omega \neq 0, 1/2$ ) with unit topological charge is composed of  $N$  dyons (magnetic monopoles) in gauge group  $SU(N)$ , namely its action density can have  $N$  peaks located at  $N$  constituent dyons when these are well separated. A picture for the action density of a  $SU(2)$  charge-one caloron is shown in Fig. 1. In  $SU(2)$ , a charge-one caloron has two constituent dyons, one has magnetic charge +1 (M dyon), another has magnetic charge -1 (L dyon), the distance between the two dyons is  $\pi\rho^2/\beta$ , where  $\rho$  is the size parameter of the caloron (and  $\beta = 1/k_B T$ ). Furthermore, one of the dyons has a twist of unit one relative to the other dyon (here, a twist is a nontrivial gauge transformation in time direction). In periodic gauge, the M dyon is approximately static while the L dyon carries a unit twist [3]. It can be shown that the topological charge of the caloron equals the magnetic charge times the relative twist of its constituent dyons [3]. In this way, calorons and magnetic monopoles are close relatives.

We will think of the traced holonomy  $\text{tr} P(\vec{x} \rightarrow \infty) = 2 \cos(2\pi\omega)$  as identified with the center symmetry order parameter  $\langle \text{tr} P \rangle$ , such that maximal nontrivial holonomy  $\omega = 1/4$  stands for the confined phase, whereas other holonomies amount to temperatures  $T > T_c$ .

Vortices and magnetic monopoles are also closely related with each other. In four dimensional space time, vortices form two dimensional world sheets while magnetic monopoles are one dimensional world lines. In the combination of Laplacian Abelian Gauge (LAG [5]) and Laplacian Center Gauge (LCG [6]), magnetic monopole worldlines reside on the vortex sheets [7].

Here we are going to find the relation between  $SU(2)$  caloron and vortices. This includes the vortices in individual calorons depending on the holonomy, the intersection of different parts of vortices recovering the topological charge and the dependence of vortices in a caloron gas on the holonomy which has an interesting relation to percolation and confinement.

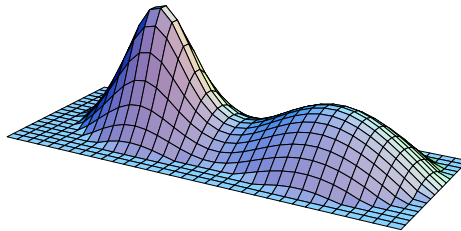


**Figure 1:** Action density of a  $SU(2)$  caloron shown in logarithmic scale, from [3].

## 2. Laplacian Center Gauge

There are different gauge fixing methods to find vortices, such as Direct Maximal Center Gauge (DMCG) [8] and Indirect Maximal Center Gauge (IMCG) [9]. An alternative is the Laplacian Center Gauge (LCG), which can be viewed as a generalization of DMCG avoiding the Gribov copy problem [6]. To this end one computes the two lowest eigenvectors  $(\phi_0, \phi_1)$  of the gauge covariant Laplace operator in the adjoint representation, which we do by virtue of ARPACK.

In LCG, the first step is to rotate the lowest mode  $\phi_0$  to the third color direction with a gauge transformation  $V$ ,  ${}^V\phi_0 = |\phi_0| \sigma_3$ , i.e. to diagonalize it. The remaining Abelian freedom of rotations around the third axis,  $V \rightarrow vV$  with  $v = \exp(i\alpha\sigma_3)$ , is fixed (up to center elements) by demanding a particular form of the first excited mode,  $({}^vV\phi_1)^{a=2} = 0$  and  $({}^vV\phi_1)^{a=1} > 0$ .

Defects of this gauge fixing appear when  $\phi_0$  and  $\phi_1$  are collinear, because then the Abelian freedom parameterized by  $v$  remains unfixed. It was shown in [6] that points  $x$  where  $\phi_0(x)$  and  $\phi_1(x)$  are collinear define the (generically two-dimensional) vortex surface. This includes points  $x$ , where  $\phi_0$  vanishes,  $\phi_0(x) = 0$ , which define monopole worldlines in the Laplacian Abelian Gauge (LAG) [5].

We detect the center vortices in LCG with the help of a topological argument: after having diagonalised  $\phi_0$  with  $V$ , the question whether  $\phi_0$  and  $\phi_1$  are collinear amounts to  ${}^V\phi_1$  being diagonal too, i.e. having zero nondiagonal components. We therefore inspect the projection of  ${}^V\phi_1$  onto the  $(\sigma_1, \sigma_2)$ -plane for all four points of each plaquette, see Fig. 2. By assuming continuity of the field on the plaquette, a nontrivial winding number of the 2d vector  $({}^V\phi_1^1, {}^V\phi_1^2)$  around the edge of the plaquette indicates a zero inside. In this case we say that the midpoint of that plaquette belongs to the vortex surfaces. The vortex sheet extends in dual directions from the midpoint. It consists of plaquettes of the dual lattice shifted by  $a/2$  in all directions with respect to the original lattice.

The first step of LCG, i.e.  ${}^V\phi_0 = |\phi_0| \sigma_3$  can include gauge transformations varying rapidly in space, this would result in artificial winding numbers and thus unphysical vortices. However, to detect vortices, the lowest eigenvector can be fixed to any direction [6], i.e. fixed to different color directions on different points. Thus, plaquette by plaquette we rotate  $\phi_0$  to its average direction over the four sites on the plaquette (which in most cases is a small rotation), afterwards we inspect  $\phi_1$  in the plane perpendicular to that direction.

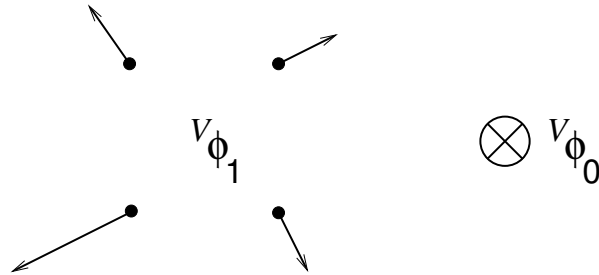


**Figure 2:** The topological argument to detect vortices on a plaquette: Components of the first excited mode  $\phi_1$  that are perpendicular to the lowest mode  $\phi_0$  (after both have been gauge transformed by  $V$ ) are plotted on all sites of the plaquette. The configuration shown here has a nontrivial winding number, which implies that the two eigenvectors are collinear in color space somewhere inside the plaquette.

### 3. Vortex Surface in a Single Caloron

To reveal the vortex surface in unit charge caloron, we discretise it on  $N_0 = 8$  and space extension  $N_i \gg 8$  lattices with constituent dyons on the  $x_3$ -axis and the center of mass fixed at the origin. After that, we compute the two lowest eigenvectors of the Laplacian operator in the adjoint representation. The lowest mode we get does not depend much on the size of the lattice, but the first excited state depends on the ratio of  $N_3$  to  $N_{1,2}$ . We find that when  $N_3/N_{1,2}$  is larger than 1 (such as 80/48), the first excited mode is a singlet, when this ratio is equal to or smaller than 1 (such as 64/64), the first excited mode is a doublet.

This ambiguity reflects the fact that we are forcing states of a continuous spectrum into a finite volume, which is similar to waves in a potential well thus sensitive to boundary conditions (such as  $N_i$ ). Gross features of the adjoint spectrum in a caloron background can be understood from the spectrum in a constant link background with the same holonomy, see [10] for details.

Using the 'local' LCG we mentioned in the last section, we find that the vortex surface in a unit charge caloron consists of two parts, a dyon charge induced part (shown in Fig. 3) and a twist induced part.

If the first excited mode belongs to a doublet, there are two vortex lines connecting the M-dyon with the L-dyon in every time slice where they exist. For large  $\rho$  caloron ( $\rho \gtrsim 0.5\beta$ ), the M-dyon and L-dyon exist in all time slices. Then the vortex sheet is completely in space-time direction. For a small  $\rho$  caloron, the monopole world line is closed and extends over a finite time interval. The vortex sheet forms a sphere that includes also space-space plaquettes. Taking another eigenvector in the doublet, the vortex lines will be rotated around the  $x_3$  axis (in all time slices). This reflects the axial symmetry of the caloron.

If the first excited mode is a singlet, on the other hand, the dyon charge induced vortex sheet

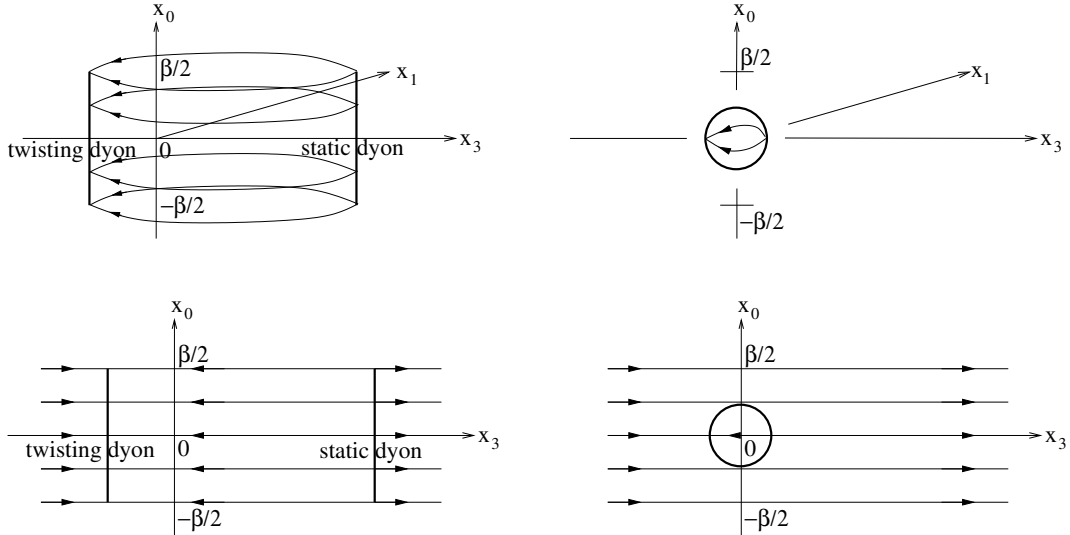


**Figure 3:** Schematic pictures for the dyon charge induced vortex part. The upper row is obtained if the first excited mode is part of a doublet. The vortex forms a tube or sphere. The lower row corresponds to the case of the first excited mode being a singlet. The vortex is spanning the  $(x_3, x_0)$ -plane. The cases of large caloron size parameters  $\rho$  are shown on the left, the small  $\rho$  cases (with closed monopole worldlines in the LAG) on the right.

is the  $(x_3, x_0)$ -plane which contains the monopole world lines. The flux on it changes its sign at the dyons. Also in this case there are two fluxes running from one of the dyons to the other.

The twist induced part of vortices in a unit charge caloron is not much different if obtained from the doublet or singlet first excited mode. We find that the shape of this part of vortices depends strongly on  $\omega$ . For maximal nontrivial holonomy calorons  $\omega = 1/4$  it is a plane between the two dyons, if  $\omega < 1/4$  it is a ‘bubble’ around the L-dyon, and if  $\omega > 1/4$  it is a bubble around the M-dyon (all at fixed time  $x_0$ ). The corresponding pictures are shown in Fig. 4. When this part of vortices is a bubble ( $\omega \neq 1/4$ ), the size of the bubble also depends on  $\rho$ , see [10].

It might be surprising that the bubble only surrounds one of the dyons while both dyons are of same importance in a caloron. This is resolved by our claim, that the bubble is (approximately) the boundary between the static region and the twist region in a caloron.

Why is that? Consider a pure twisting-static configuration which mimics the twist:

$$A_0(t, \vec{x}) = \begin{cases} \pi\sigma_3/\beta & \text{for } \vec{x} \in S \\ 0 & \text{for } \vec{x} \notin S \end{cases} \quad A_i(t, \vec{x}) = 0, \quad (3.1)$$

where  $S \subset \mathbf{R}^3$  is the twist region. We recall that vortices are signalled by contractible closed  $-1_2$

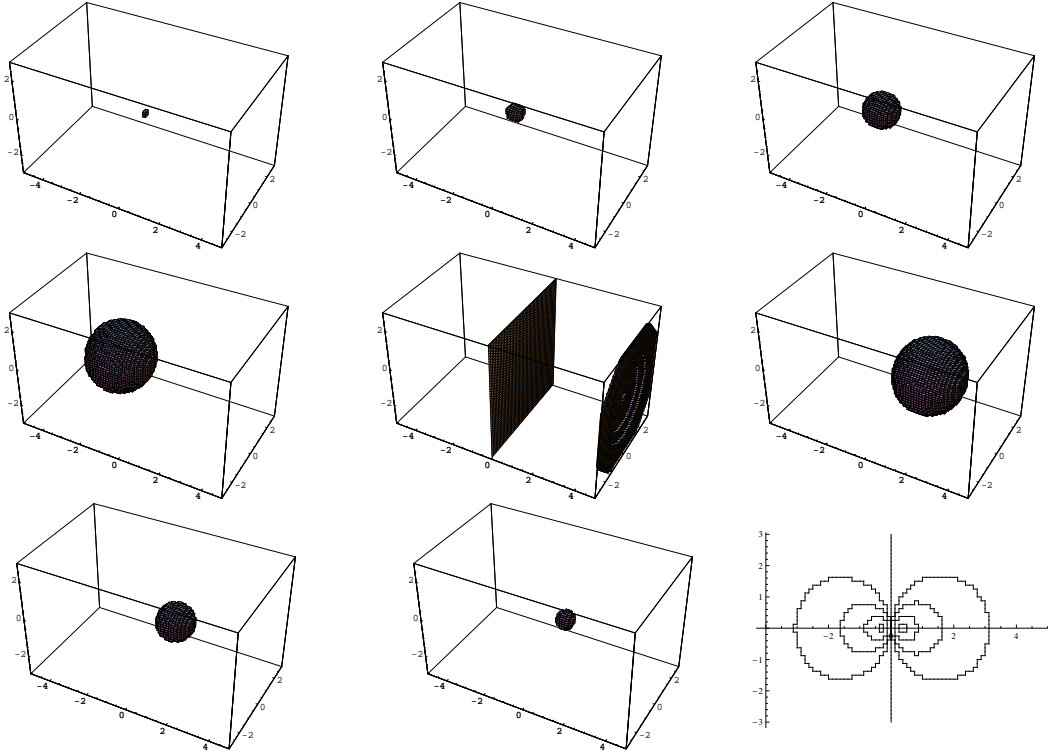


**Figure 4:** Twist induced part of the vortices (‘bubble’) from singlet first excited modes for calorons of size  $\rho = 0.6\beta$  in  $(x_1, x_2, x_3)$  subspace (a time slice) and plotted in units of  $\beta$ . Holonomies from left to right:  $\omega = 0.1, 0.12, 0.16$  (upper row)  $\omega = 0.2, 0.25, 0.3$  (middle row) and  $\omega = 0.34, 0.38$  (lower row, left panel). The plot in the lower right corner summarizes the results for  $\omega = 0.10, 0.12, 0.16, 0.20, 0.25, 0.30, 0.34, 0.38, 0.40$  in a two-dimensional plot at  $x_1 = 0$ . The plane near the boundary in the  $\omega = 0.25$  picture is an artifact caused by periodic boundary conditions.

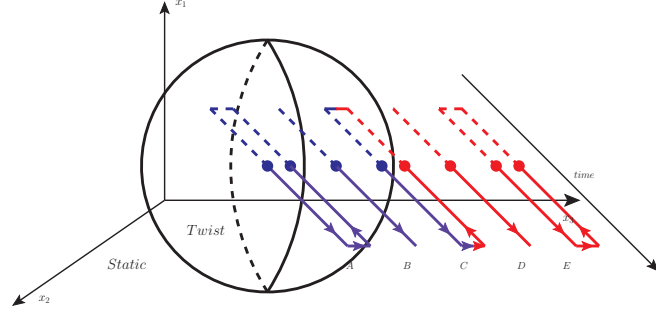


**Figure 5:** Different contours in a pure twisting-static configuration, see text.

loops. We consider different contours as shown in Fig. 5. Loops within the static region (like D, a Polyakov loop, or E) or contractible loops within twist region (like A) are trivial. On the other hand, some loops giving  $-1_2$  within twist region (like B, a Polykov loop) are non-contractible. Only loops that cross the twist *and* static region (like C) are  $-1_2$  and contractible, hence enclose the vortex surface. It shows that the vortex surface in this configuration is in space-space direction, it is the 2d boundary between different twists, the time coordinate is not fixed by this argument.

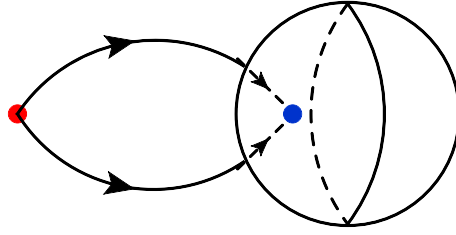


**Figure 6:** The intersection of the vortices in a caloron at fixed  $x_0$  coordinate. Dots indicate the dyons (monopoles in the LAG).

The dyon charge induced vortex surface in the case of large  $\rho$  is completely in space-time direction, while the twist induced vortices is in space-space direction. These two kinds of vortices always have two intersection points as shown in Fig. 6. Each of these points gives topological charge<sup>1</sup>  $1/2$ , and this recovers the topological charge of the caloron. The general relation of vortices with topological charge has been worked out in [11].

#### 4. Vortex Surface in Caloron Gases

The caloron ensembles considered in this paper have been created along the lines of Ref. [12]. The 4 dimensional center of mass locations of the calorons and anticalorons are sampled randomly as well as the spatial orientation of the ‘dipole axis’ connecting the two dyons and the angle of a global  $U(1)$  rotation around the axis  $\omega\sigma^3$  in color space. The caloron size is sampled from a suitable size distribution  $D(\rho, T)$ .

Suppose the vortex distribution in a dilute caloron gas forms by a recombination of the vortices of single calorons, see Fig.7. Then for a caloron gas with holonomy  $\omega \neq 1/4$  the space-space

<sup>1</sup>As well known, an intersection point can contribute topological charge  $\pm 1/2$ .

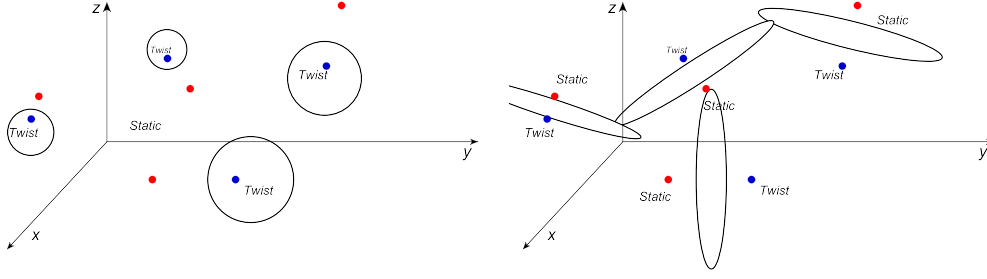


**Figure 7:** Recombination of vortices in caloron gases (schematically) for holonomy parameters  $\omega \neq 1/4$  (left) and maximal nontrivial holonomy  $\omega = 1/4$  (right).

directed vortices should be separated bubbles, a bubble for each caloron (if these bubbles are not too close or too large to touch each other). But the situation in a caloron gas with maximal nontrivial holonomy  $\omega = 1/4$  is completely different. The space-space directed vortices in every single caloron form a plane that tends to extend to infinity. In the result, the vortices of different calorons touch each other and recombine to form a percolating surface. This scenario is rather independent of the caloron density or temperature.

We recall that vortices give a linear potential only when they percolate. Percolation means the sizes of some of the vortices clusters are comparable to the size of the lattice. Several papers have reported percolation of vortex clusters in Monte Carlo simulated configurations below the critical temperature [13].

Numerical results for vortices in caloron ensembles with different holonomy are shown in Fig. 8. These configurations have their calorons located at the same random coordinates, in the same direction and with the same  $\rho$  parameters, the only varying parameter is the holonomy  $\omega$ . It can be seen clearly that space-space directed vortices only in the maximally nontrivial holonomy case form percolating clusters, while the space-time directed vortices percolate independently of  $\omega$ . Thus calorons induce confinement for  $\omega = 1/4$  and a constant string tension of spatial Wilson loops. Our results via center vortices agree with other caloron studies showing a similar holonomy-dependence of confinement manifesting itself in Polyakov correlators [14, 12].

## 5. Conclusion

Using Laplacian Center Gauge, we find that the vortices in a  $SU(2)$  caloron include two parts: the constituent dyon charge induced part and the twist induced part. The latter part is mainly in space-space direction and percolates in a caloron ensemble in the case of maximal nontrivial holonomy. Under our conjecture this amounts to the confined phase with vanishing Polyakov loop. We have demonstrated that this behavior can be understood from the dependence of the vortex shape on the holonomy in individual calorons. This finding fits perfectly in the confinement scenarios of vortices and shows that calorons are suitable to facilitate the vortex confinement mechanism.

This work has been supported by DFG (BR 2872/4-1).

## References

- [1] P. Y. Boyko *et al.*, Nucl. Phys. B **756**, 71 (2006) [hep-lat/0607003]; V. G. Bornyakov *et al.*, Phys. Rev. D **77**, 074507 (2008) [0708.3335 [hep-lat]].

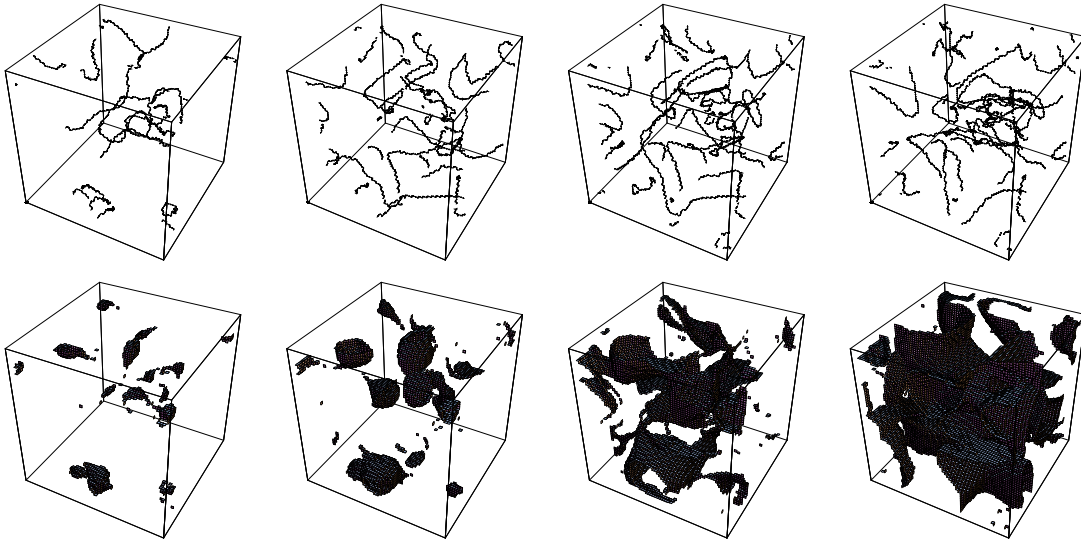


**Figure 8:** Vortices in caloron gas configurations. The first row are space-time direction vortices traced out within the box representing the first time slice. The second row are space-space direction vortices from all time slices overlaid in one spatial box. The holonomy parameter  $\omega$  of the (anti)calorons is 0.0625, 0.125, 0.1875 and 0.25 from left to right.

- [2] B. J. Harrington, H. K. Shepard, *Phys. Rev. D* **17** (1978) 2122.
- [3] T. C. Kraan, P. van Baal, *Nucl. Phys. B* **533** (1998) 627 [hep-th/9805168].
- [4] K. M. Lee, C. h. Lu, *Phys. Rev. D* **58** (1998) 025011 [hep-th/9802108].
- [5] A. J. van der Sijs, *Nucl. Phys. Proc. Suppl.* **53** (1997) 535 [hep-lat/9608041]; *Prog. Theor. Phys. Suppl.* **131** (1998) 149 [hep-lat/9803001].
- [6] P. de Forcrand, M. Pepe, *Nucl. Phys. B* **598** (2001) 557 [hep-lat/0008016].
- [7] C. Alexandrou, M. D'Elia, P. de Forcrand, *Nucl. Phys. Proc. Suppl.* **83** (2000) 437 [hep-lat/9907028].
- [8] L. Del Debbio *et al.*, *Phys. Rev. D* **58**, 094501 (1998) [hep-lat/9801027]
- [9] L. Del Debbio, M. Faber, J. Greensite, S. Olejnik, *Phys. Rev. D* **55**, 2298 (1997) [hep-lat/9610005]
- [10] F. Bruckmann, E.-M. Ilgenfritz, B. V. Martemyanov, Bo Zhang, in preparation.
- [11] M. Engelhardt, *Nucl. Phys. B* **585** (2000) 614 [hep-lat/0004013]; H. Reinhardt, *Nucl. Phys. B* **628** (2002) 133 [hep-th/0112215]; M. Engelhardt, H. Reinhardt, *Nucl. Phys. B* **567** (2000) 249 [hep-th/9907139]; F. Bruckmann, M. Engelhardt, *Phys. Rev. D* **68** (2003) 105011 [hep-th/0307219].
- [12] P. Gerhold, E.-M. Ilgenfritz, M. Müller-Preussker, *Nucl. Phys. B* **760** (2007) 1 [hep-ph/0607315].
- [13] M. Engelhardt, K. Langfeld, H. Reinhardt, O. Tennert, *Phys. Rev. D* **61** (2000) 054504 [hep-lat/9904004]; M. Engelhardt, H. Reinhardt, *Nucl. Phys. B* **585** (2000) 591-613 [hep-lat/9912003]; J. Greensite, *Prog. Part. Nucl. Phys.* **51** (2003) 1 [hep-lat/0301023].
- [14] E.-M. Ilgenfritz *et al.*, PoS LAT2005:306,2006. [hep-lat/0509171]